Supporting Information

1. Materials and Instruments Methods

Tris(4-aminophenyl)amine(97%),1,4-Benzenedicarboxaldehyde(98%)and 4,4'-Biphenyl dicarboxaldehyde(98%) were purchased from Shanghai Yuanye Biotechnology Co., Ltd. 1,3,5-Trimethylbenzene was purchased from TCI Chemicals. Acetone (AR), absolute ethanol (CP) and acetic acid (CP) were all purchased from Sinopharm Chemical Reagent Co., Ltd.

X-ray photoelectron spectrometer (Thermo Scientific ESCAlab 250xi); ultraviolet-visible spectrophotometer (UV-3600); Fourier transform infrared spectroscopy absorber (Thermo Nicolet Is10); atomic force microscope (Bruker Dimension Edge);Semiconductor Tester (B1500A); Quad Probe Station; Field Emission Scanning Electron Microscope (JSM-7100f); High Vacuum Metal Evaporation Analyzer (Quorum Q150t).

2. Computational details

Our first-principle calculations were performed using VASP code[1], based on density-functional theory (DFT) [2,3] and Heyd-Scuseria-Ernzerhof(HSE06) hybrid functional [4]. The effect of van der Waals interactions was estimated, implemented in the optimized exchange van der Waals functional DFT-D3[5]. The plane wave cutoff energy was 500 eV and the k-point meshes of 1×1×1 and 3×3×1 in the Monkhorst Pack[6] sampling scheme were used for geometry optimization and electronic self-consistent computation, respectively. The convergence condition for the energy was 10^{-4} eV, and the structures were relaxed until the force on each atom was less than 0.01 eV/Å. Spin polarization was considered in all calculations. And the structure drawing and charge density visualization were generated using VESTA[7].

3. Synthesis Procedure

3.1 The preparation of TT-COF and BT-COF powder.

TT-COF: Take 10.4mg of Tris(4-aminophenyl) amine(0.03581mmol) in a clean glass bottle A, then add 5ml of ethanol, 5ml and 1ml of acetic acid, stir at room temperature for 30min for reserve. Take 4.8mg of 1,4-Benzenedicarboxaldehyde(0.03579mmol) into a clean glass bottle A, and then add 2.5ml of ethanol, 2.5ml and 500μl of acetic acid, stir for 30min at room temperature for reserve. Mix the solution in bottles A and B and let stand for the reaction at room temperature for 20 min. The precipitated products after the reaction are collected by filtration and washed with absolute ethanol until the ethanol is colorless after washing. Finally, it is dried in a drying oven at 60℃ for 12h to obtain red powder.

BT-COF: Take 10.4mg of Tris (4-aminophenyl) amine(0.03581mmol) in a clean glass bottle A , then add 5ml of ethanol, 5ml and 1ml of acetic acid, stir at room temperature for 30min for reserve. Take 7.5mg of 4,4'-Biphenyldicarboxaldehyde(0.03567mmol) into a clean glass bottle B, and then add 4ml of ethanol, 4ml and 800μl of acetic acid, stir for 30min at room temperature for reserve. Mix the solution in bottles A and B and let stand for the reaction at room temperature for 20 min. The precipitated products after the reaction are collected by filtration and washed with absolute ethanol until the ethanol is colorless after washing. Finally, it is dried in a drying oven at 60℃ for 12h to obtain orange powder.

3.2 Specific process for growing covalent organic framework (TT-COF and BT-COF) films in situ on ITO.

1)Cleaning process of the substrate

We use a SiO_2 substrate with a 100nm thick ITO of 2cm*2cm*1mm. First, put the substrate in deionized water, add detergent powder to soak for 1h, then rinse off the surface stains, and use ultrapure water, absolute ethanol, isopropanol acetone ultrasonic cleaning for 30min. Finally, the cleaned substrate was dried in a drying oven at 60°C for 6h for later use**.**

2)Configure the monomer solution

TT-COF: Take 3.2mg of Tris (4-aminophenyl) amine(0.01102mmol) in a clean glass bottle A , then add 1.5ml of ethanol, 1.5ml and 300μl of acetic acid, stir at room temperature for 30min for reserve. Take 4.8mg of 1,4-Benzenedicarboxaldehyde(0.03579mmol) into a clean glass bottle B, and then add 2.5ml of ethanol, 2.5ml and 500μl of acetic acid, stir for 30min at room temperature for reserve.

BT-COF: Take 3mg of Tris (4-aminophenyl) amine(0.01033mmol) in a clean glass bottle A, then add 5ml of ethanol, 5ml and 1ml of acetic acid, stir at room temperature for 30min for reserve. Take 5.2mg of 4,4'-Biphenyldicarboxaldehyde(0.02473mmol) into a clean glass bottle B, and then add 2.5ml of ethanol, 2.5 ml and 500 μl of acetic acid, stir for 30min at room temperature for reserve.

3)In situ growth of covalent organic frameworks films

Mix the solution in equal volumes of A and B bottles and add 200 μl of the mixture dropwise with a pipette onto a substrate placed on a horizontal plane. After waiting for its reaction for 8 min, rinse off the unfinished solution and some unfilmed precipitate with absolute ethanol. After that, the cleaned devices are put into a drying oven at 60°C and dried for 6h.

4. Device Fabricationand Performance Test Methods

The specific process of preparing the memristors are as follows: starting from cleaning the substrate; The films are then grown in situ on the substrate (the specific procedure is shown in Section 3.2); then a 100 nm Al electrodes are prepared in a vacuum evaporator using a homemade mask plate. The *I-V* curve, cyclic stability test curve, hold time, and drive voltage distribution of memristors were all tested on the B1500A.

5. Supporting Figures and Legends for as-obtained materials

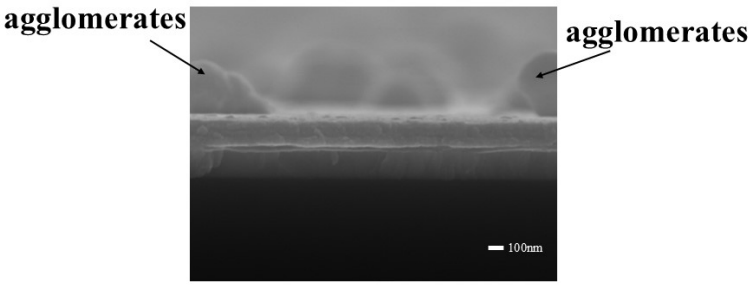

Figure S1. Cross section FE-SEM image of Al/TT-COF/ITO memristor based on reaction time to 20 minutes.

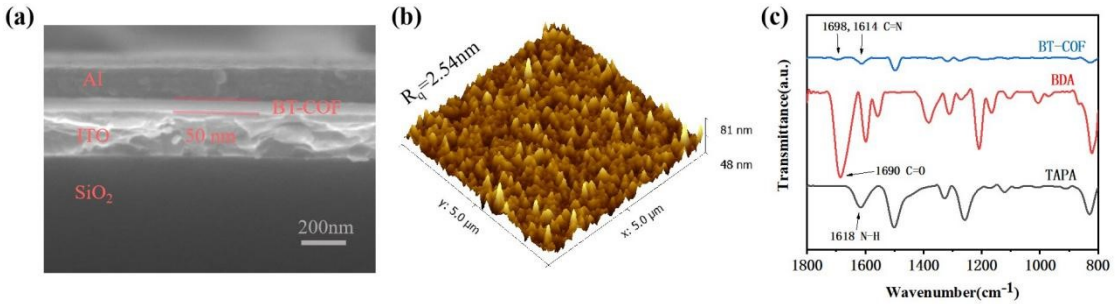

Figure S2.a) Cross section FE-SEM images of Al/BT-COF/ITO memristors; **b)** AFM 3D image of BT-COF; **c)** FT-IR spectrum of BT-COF, BDA and TAPA.

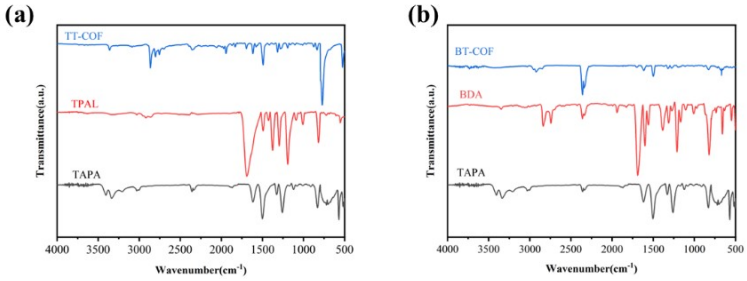

Figure S3. a) FT-IR spectrum of TT-COF, TPAL and TAPA; **b)** FT-IR spectrum of BT-COF, BDA and TAPA.

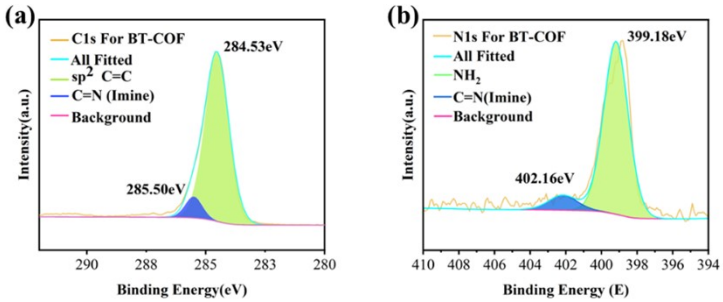

Figure S4.XPS spectra of BT-COF. **a)** C1s core level; **b)** N1s core level;

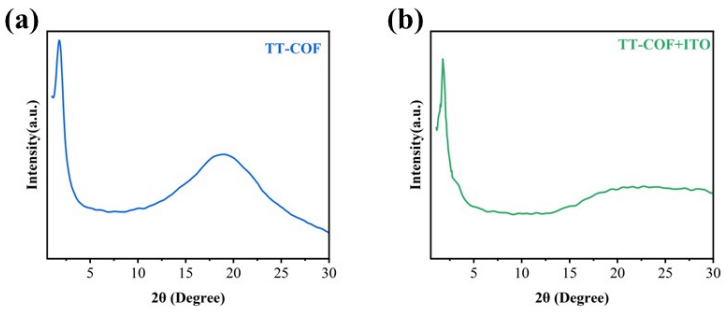

Figure S5. XRD pattern of synthesized TT-COF a) powder form and b) thin film form.

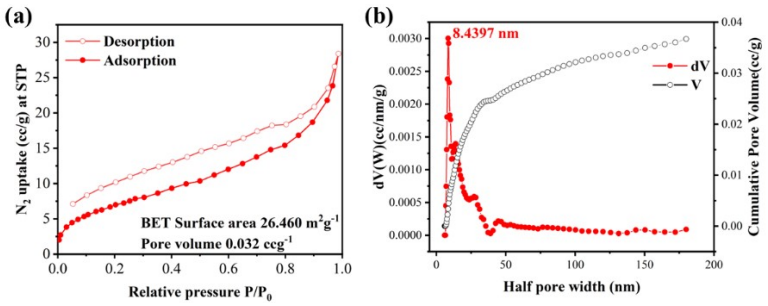

Figure S6. a) Brunauer–Emmett–Teller(BET)surface areas determined by N2 sorption isotherms measured at 77 K ;**b)** Pore-size distribution (PSD) as measured by NLDFT method.

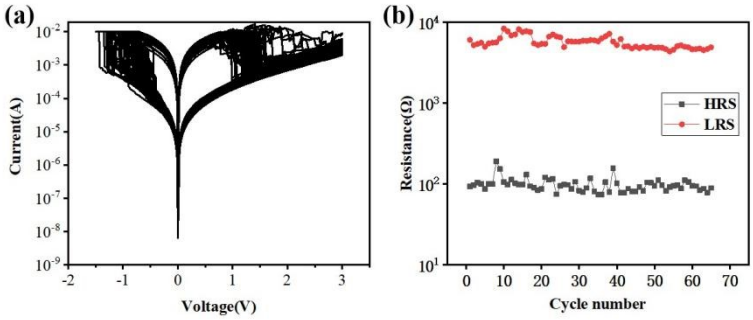

Figure S7. a) Current-voltage characteristics and **b)** Cyclic resistance distribution of Al/BT-COF/ITO memristor.(Negative scan SET)

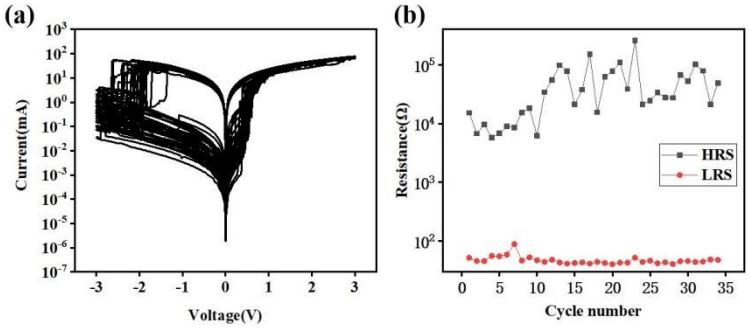

Figure S8.a) Current-voltage characteristics and **b)** Cyclic resistance distribution of Al/BT-COF/ITO memristor .(Positive scan SET)

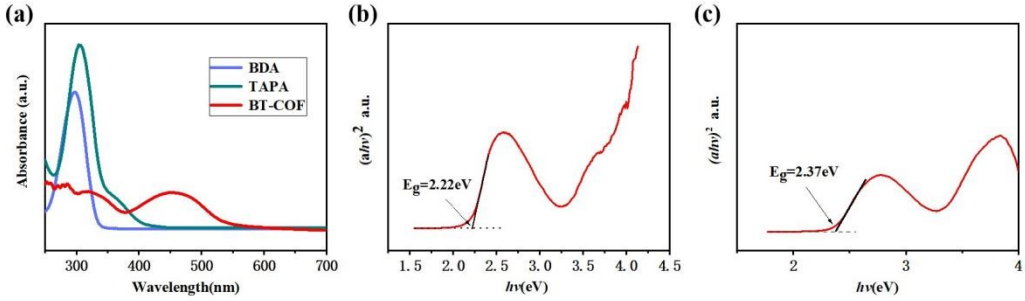

Figure S9.a) UV−visible absorption spectra of the BT-COF film, TAPA, and BDA; **b)** Tauc plot deriving from the UV-visible light absorption spectrum of TT-COF and **c)** BT-COF

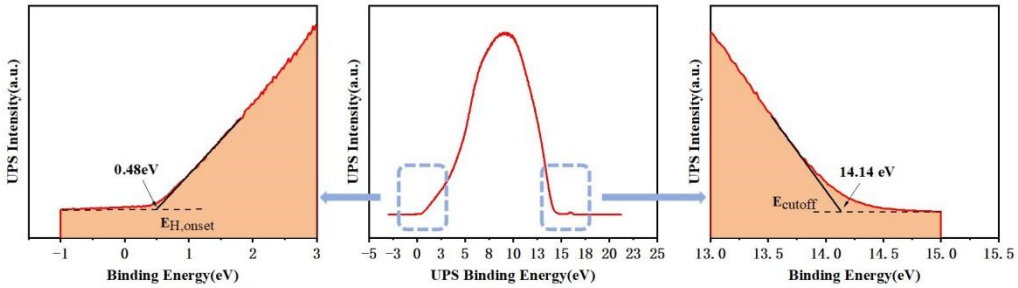

Figure S10.UPS spectra of the BT-COF thin film.

The HOMO energy levels are calculated as follows $\mathbf{IPs} = h\nu - (E_{cutoff} - E_{H,onset})$, thus, HOMO energy level for TT-COF and BT-COF is -5.10 and -4.66 eV, respectively.

The LUMO energy levels are calculated as follows $E_{LUMO} = E_{HOMO}$**, UPS +** E_g**,** thus, LUMO energy level for TT-COF and BT-COF is -2.88 and -2.29 eV, respectively[8,9].

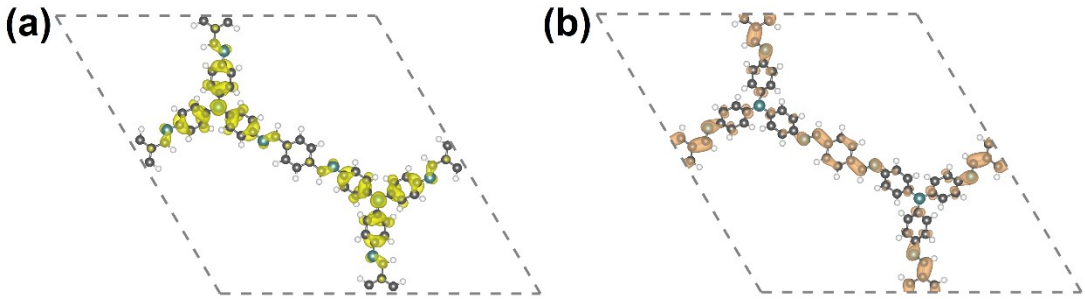

Figure S11. The partial charge densities for the (a) HOMO and (b) LUMO of TT-COF. Isosurface level is set to be 0.001 e Å^{-3}. The grey, green and white balls are C, N and H, respectively.

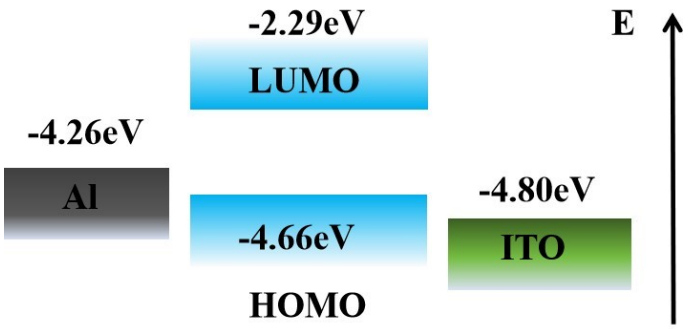

Figure S12 Band diagrams and relative levels of BT-COF films compared to ITO and Al electrodes.

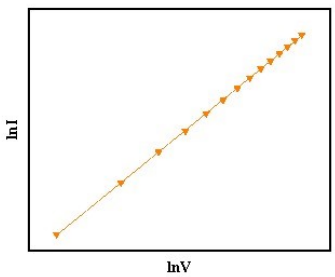

Figure S13. ln*I* vs. ln*V* plot in the HRS on the negative scan.

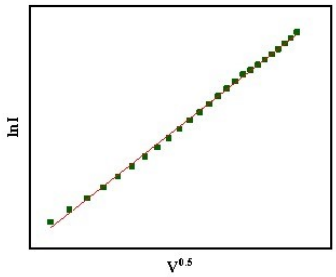

Figure S14. Schottky emission fitting plot in the LRS on the negative scan.

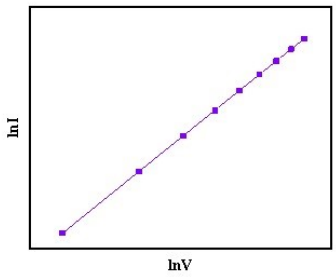

Figure S15. ln*I* vs. ln*V* plot in the LRS on the negative scan.

Table S1 Performance comparison of nonvolatile resistive switching memristors

Active layer	Device configuration	Type	Switching mechanism	Turn-on voltage (V)	ON/OFF current ratio	Retention time(*10^3s)	Endurance (cycles)	Ref
2D COFs								
$2DP_{BTA+PDA}$	Ag/$2DP_{BTA+PDA}$(71 nm)/ITO	Rewritable (Bipolar)	Filament mechanism	+0.90	~10^5	35	200	[10]
PI-NT	Al/ PI-NT (90-150 nm)/LiF(1 nm)/ITO	WORM (Bipolar)	Electric-field-induced charge transfer	+2.30 / −2.64	Over 10^6	10	200	[11]
COF-TT-BT	Ag/COF-TT-BT (100 nm)/ ITO	Rewritable (Bipolar)	Filament mechanism	+1.30	~10^5	33	319	[12]
COF-Azu	Al/COF-Azu(160nm)/ITO	Rewritable (Bipolar)	Electric-field-induced charge transfer	+1.95/-0.5	50	30	300	[13]
COF-EtD	ITO/COF-EtD/Ag	Rewritable (Bipolar)	SCLC/Ag Filament mechanism	-2.1	10^4	10	280	[14]
TT-COF	Al/TT-COF(51nm)/ITO	Rewritable (Bipolar)	Electric-field-induced charge transfer	+0.8/-0.8	Over 10^2	10	550	This work

Table S2 Unit cell parameters and fractional atomic coordinates for TT-COF

COF Space group:'P1' ;

a=32.09781 Å, b=32.32804 Å, c=30.00000 Å;

α = β = 90° , γ = 120.7023°

label	symbol	x	y	z
C1	C	0.44404	0.90093	0.47901
C2	C	0.63734	0.28599	0.48399
C3	C	0.59384	0.26275	0.50846
C4	C	0.564	0.21311	0.50649
C5	C	0.57724	0.18471	0.48145
C6	C	0.6206	0.20831	0.45653
C7	C	0.64991	0.25805	0.45754
C8	C	0.4749	0.9531	0.47725
C9	C	0.52584	0.97604	0.47627
C10	C	0.45321	0.98164	0.4773
C11	C	0.10655	0.54323	0.47937
C12	C	0.71853	0.35759	0.48508
C13	C	0.74061	0.33707	0.51001
C14	C	0.79046	0.3569	0.50866
C15	C	0.82033	0.39893	0.48388
C16	C	0.7979	0.41926	0.45889
C17	C	0.74792	0.39875	0.45919
C18	C	0.05426	0.52308	0.47811
C19	C	0.03399	0.55282	0.47787
C20	C	0.02292	0.4727	0.47808
C21	C	0.4636	0.56522	0.4807
C22	C	0.6471	0.36628	0.48474
C23	C	0.66796	0.40905	0.50985
C24	C	0.64857	0.43879	0.50836
C25	C	0.60662	0.42614	0.48322
C26	C	0.58608	0.38338	0.45786
C27	C	0.60618	0.35419	0.45833
C28	C	0.48313	0.53321	0.47941
C29	C	0.45278	0.48277	0.4791
C30	C	0.5338	0.55305	0.47904
C31	C	0.56306	0.1066	0.47845
C32	C	0.36959	0.72135	0.48331
C33	C	0.41314	0.74446	0.50773
C34	C	0.443	0.79412	0.5061
C35	C	0.42974	0.82275	0.48148
C36	C	0.38624	0.79931	0.45673
C37	C	0.35694	0.74956	0.45735
C38	C	0.53219	0.0544	0.47696
C39	C	0.48123	0.03146	0.47722
C40	C	0.55386	0.02585	0.47611

C41	C	0.90053	0.46235	0.48071
C42	C	0.28845	0.6495	0.48364
C43	C	0.26591	0.66961	0.50846
C44	C	0.21601	0.64937	0.50696
C45	C	0.18651	0.60729	0.48212
C46	C	0.20937	0.58746	0.45708
C47	C	0.25942	0.60841	0.45753
C48	C	0.95275	0.48223	0.47894
C49	C	0.973	0.45248	0.47854
C50	C	0.98411	0.5326	0.47824
C51	C	0.54304	0.44146	0.48047
C52	C	0.35996	0.64102	0.48399
C53	C	0.33886	0.59824	0.50906
C54	C	0.35816	0.56841	0.50783
C55	C	0.40029	0.58097	0.48301
C56	C	0.42114	0.62382	0.45774
C57	C	0.40109	0.65306	0.45792
C58	C	0.52335	0.47332	0.47919
C59	C	0.5537	0.52375	0.47898
C60	C	0.47268	0.45346	0.47891
N1	N	0.87008	0.41682	0.48422
N2	N	0.58887	0.45749	0.48376
N3	N	0.54601	0.13498	0.48175
N4	N	0.33943	0.6707	0.48418
N5	N	0.13668	0.58886	0.48258
N6	N	0.4178	0.54942	0.4837
N7	N	0.66759	0.33661	0.48527
N8	N	0.46104	0.87247	0.48182
H1	H	0.40456	0.887	0.479
H2	H	0.58362	0.2841	0.52882
H3	H	0.53023	0.19497	0.52533
H4	H	0.63029	0.18741	0.43487
H5	H	0.68281	0.2759	0.43745
H6	H	0.54241	0.95383	0.47607
H7	H	0.41371	0.96397	0.47775
H8	H	0.11886	0.51689	0.47872
H9	H	0.71814	0.30514	0.53009
H10	H	0.80765	0.34091	0.52769
H11	H	0.81992	0.45029	0.43755
H12	H	0.73101	0.4141	0.43884
H13	H	0.05835	0.59171	0.47775
H14	H	0.03846	0.44949	0.47809
H15	H	0.4907	0.60421	0.48011
H16	H	0.69978	0.41883	0.53027

H17	H	0.66481	0.47206	0.52758
H18	H	0.5552	0.3741	0.4362
H19	H	0.59064	0.32184	0.43779
H20	H	0.41366	0.46759	0.47921
H21	H	0.5575	0.59213	0.47905
H22	H	0.60254	0.12057	0.47789
H23	H	0.42342	0.72298	0.52783
H24	H	0.47677	0.81207	0.52494
H25	H	0.37645	0.82039	0.4354
H26	H	0.32402	0.73193	0.43728
H27	H	0.46467	0.05368	0.47768
H28	H	0.59336	0.04352	0.47568
H29	H	0.88853	0.48895	0.48006
H30	H	0.28806	0.70154	0.52865
H31	H	0.19851	0.66508	0.52596
H32	H	0.18764	0.55644	0.43565
H33	H	0.27665	0.59337	0.4372
H34	H	0.94864	0.41359	0.47897
H35	H	0.96858	0.55582	0.47828
H36	H	0.51609	0.40243	0.47971
H37	H	0.3069	0.58849	0.52926
H38	H	0.34168	0.53511	0.52703
H39	H	0.45219	0.63309	0.43633
H40	H	0.41685	0.68543	0.4374
H41	H	0.59282	0.53892	0.47905
H42	H	0.44898	0.41437	0.47882

References

[1] G. KRESSE, J. HAFNER, AB-INITIO MOLECULAR-DYNAMICS SIMULATION OF THE LIQUID-METAL AMORPHOUS-SEMICONDUCTOR TRANSITION IN GERMANIUM, PHYSICAL REVIEW B 49 (1994) 14251–14269. https://doi.org/10.1103/PhysRevB.49.14251.

[2] P. HOHENBERG, W. KOHN, INHOMOGENEOUS ELECTRON GAS, PHYSICAL REVIEW B 136 (1964) B864-+. https://doi.org/10.1103/PhysRev.136.B864.

[3] W. KOHN, L. SHAM, SELF-CONSISTENT EQUATIONS INCLUDING EXCHANGE AND CORRELATION EFFECTS, PHYSICAL REVIEW 140 (1965) 1133-. https://doi.org/10.1103/PhysRev.140.A1133.

[4] J. Heyd, G. E. Scuseria, M. Ernzerhof, J. Chem. Phys. 2003, 118, 8207.

[5] S. Grimme, J. Antony, S. Ehrlich, H. Krieg, A consistent and accurate ab initio parametrization of density functional dispersion correction (DFT-D) for the 94 elements H-Pu, JOURNAL OF CHEMICAL PHYSICS 132 (2010). https://doi.org/10.1063/1.3382344.

[6] H. MONKHORST, J. PACK, SPECIAL POINTS FOR BRILLOUIN-ZONE INTEGRATIONS, PHYSICAL REVIEW B 13 (1976) 5188–5192. https://doi.org/10.1103/PhysRevB.13.5188.

[7] K. Momma, F. Izumi, VESTA:: a three-dimensional visualization system for electronic and structural analysis, JOURNAL OF APPLIED CRYSTALLOGRAPHY 41 (2008) 653–658. https://doi.org/10.1107/S0021889808012016.

[8] T. Zhang, Y. Hou, V. Dzhagan, Z. Liao, G. Chai, M. Löffler, D. Olianas, A. Milani, S. Xu, M. Tommasini, D. Zahn, Z. Zheng, E. Zschech, R. Jordan, X. Feng, Copper-surface-mediated synthesis of acetylenic carbon-rich nanofibers for active metal-free photocathodes, NATURE COMMUNICATIONS 9 (2018). https://doi.org/10.1038/s41467-018-03444-0.

[9] C. Li, D. Li, W. Zhang, H. Li, G. Yu, Towards High-Performance Resistive Switching Behavior through Embedding a D-A System into 2D Imine-Linked Covalent Organic Frameworks, ANGEWANDTE CHEMIE-INTERNATIONAL EDITION 60 (2021) 27135–27143. https://doi.org/10.1002/anie.202112924.

[10] J. Liu, F. Yang, L. Cao, B. Li, K. Yuan, S. Lei, W. Hu, A Robust Nonvolatile Resistive Memory Device Based on a Freestanding Ultrathin 2D Imine Polymer Film, ADVANCED MATERIALS 31 (2019). https://doi.org/10.1002/adma.201902264.

[11] B. Sun, X. Li, T. Feng, S. Cai, T. Chen, C. Zhu, J. Zhang, D. Wang, Y. Liu, Resistive Switching Memory Performance of Two-Dimensional Polyimide Covalent Organic Framework Films, ACS APPLIED MATERIALS & INTERFACES 12 (2020) 51837–51845. https://doi.org/10.1021/acsami.0c15789.

[12] C. Li, D. Li, W. Zhang, H. Li, G. Yu, Towards High-Performance Resistive Switching Behavior through Embedding a D-A System into 2D Imine-Linked Covalent Organic Frameworks, ANGEWANDTE CHEMIE-INTERNATIONAL EDITION 60 (2021) 27135–27143. https://doi.org/10.1002/anie.202112924.

[13] Z. Zhao, M. El-Khouly, Q. Che, F. Sun, B. Zhang, H. He, Y. Chen, Redox-Active Azulene-based 2D Conjugated Covalent Organic Framework for Organic Memristors, ANGEWANDTE CHEMIE-INTERNATIONAL EDITION 62 (2023). https://doi.org/10.1002/anie.202217249.

[14] H. Yu, P. Zhou, X. Chen, Intramolecular Hydrogen Bonding Interactions Induced Enhancement in Resistive Switching Memory Performance for Covalent Organic Framework-Based Memristors, ADVANCED FUNCTIONAL MATERIALS 33 (2023). https://doi.org/10.1002/adfm.202308336.